

Combining quasielastic neutron scattering and molecular dynamics to study methane motions in ZSM-5

Cite as: J. Chem. Phys. **157**, 184702 (2022); <https://doi.org/10.1063/5.0123434>

Submitted: 30 August 2022 • Accepted: 21 October 2022 • Accepted Manuscript Online: 21 October 2022 • Published Online: 08 November 2022

Published open access through an agreement with JISC Collections

 Alexander P. Hawkins,  Andrea Zachariou,  Ian P. Silverwood, et al.



View Online



Export Citation



CrossMark

ARTICLES YOU MAY BE INTERESTED IN

[Adsorption of simple gases into the porous glass MCM-41](#)

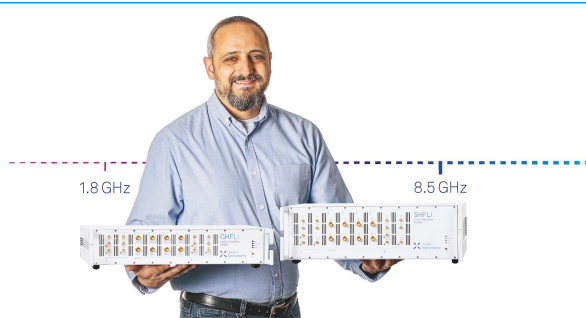
The Journal of Chemical Physics **154**, 184503 (2021); <https://doi.org/10.1063/5.0053555>


[A general method for calculating solid/liquid interfacial free energies from atomistic simulations: Application to \$\text{CaSO}_4 \cdot x\text{H}_2\text{O}\$](#)

The Journal of Chemical Physics **157**, 084117 (2022); <https://doi.org/10.1063/5.0095130>


[Phase diagram of the TIP4P/Ice water model by enhanced sampling simulations](#)

The Journal of Chemical Physics **157**, 054504 (2022); <https://doi.org/10.1063/5.0097463>



Trailblazers. 

Meet the Lock-in Amplifiers that measure microwaves.

 Zurich Instruments [Find out more](#)

Combining quasielastic neutron scattering and molecular dynamics to study methane motions in ZSM-5

Cite as: J. Chem. Phys. 157, 184702 (2022); doi: 10.1063/5.0123434

Submitted: 30 August 2022 • Accepted: 21 October 2022 •

Published Online: 8 November 2022



Alexander P. Hawkins,^{1,2} Andrea Zachariou,^{1,2} Ian P. Silverwood,^{2,6} Chin Yong,³ Paul Collier,⁴ Ilian Todorov,³ Russell F. Howe,⁵ Stewart F. Parker,^{2,6} and David Lennon^{1,a)}

AFFILIATIONS

¹ School of Chemistry, University of Glasgow, Joseph Black Building, Glasgow G12 8QQ, United Kingdom

² UK Catalysis Hub, Research Complex at Harwell, STFC Rutherford Appleton Laboratory, Chilton, Oxon OX11 0FA, United Kingdom

³ Scientific Computing Department, STFC Daresbury Laboratory, Sci-Tech Daresbury, Warrington WA4 4AD, United Kingdom

⁴ Johnson Matthey Technology Centre, Blounts Court, Sonning Common, Reading RG4 9NH, United Kingdom

⁵ Department of Chemistry, University of Aberdeen, Aberdeen AB24 3UE, United Kingdom

⁶ ISIS Neutron and Muon Facility, STFC Rutherford Appleton Laboratory, Chilton, Oxon OX11 0QX, United Kingdom

^{a)} Author to whom correspondence should be addressed: David.Lennon@glasgow.ac.uk

ABSTRACT

Quasi-elastic neutron scattering (QENS) and molecular dynamics (MD) simulations are applied in combination to investigate the dynamics of methane in H-ZSM-5 zeolite catalysts used for methanol-to-hydrocarbons reactions. Methane is employed as an inert model for the methanol reaction feedstock, and studies are made of the fresh catalyst and used catalysts with varying levels of coke buildup to investigate the effect of coking on reactant mobility. Measurements are made in the temperature range from 5 to 373 K. Methane mobility under these conditions is found to be extremely high in fresh ZSM-5, with the majority of movements occurring too fast to be resolved by the QENS instrument used. A small fraction of molecules undergoing jump diffusion on QENS time scales is identified and found to correspond with short-range jump diffusion within single zeolite pores as identified in MD simulations. Agreement between QENS and MD mobility measurements is found to be within 50%, validating the simulation approach employed. Methane diffusion is found to be minimally affected by moderate levels of coke buildup, while highly coked samples result in the confinement of methane to single pores within the zeolite with minimal long-range diffusion.

© 2022 Author(s). All article content, except where otherwise noted, is licensed under a Creative Commons Attribution (CC BY) license (<http://creativecommons.org/licenses/by/4.0/>). <https://doi.org/10.1063/5.0123434>

I. INTRODUCTION

The Methanol-to-Hydrocarbons (MTH) reaction has gained both industrial and academic traction in recent years as it uses zeolite catalysts to selectively convert methanol to high-value hydrocarbon products through a shape-selective hydrocarbon pool mechanism.^{1,2} This mechanism is widely accepted for steady state conditions although the steps leading to the formation of the first hydrocarbons and the eventual catalyst deactivation are still not well understood.^{1,2} In catalytic reactions, the diffusion and adsorption of both reactants

and products play an important role in the mechanistic understanding of the reaction, product distribution, and catalytic lifetime. The diffusion of the methanol reagent through the zeolite at different life cycle stages affects the selectivity and, therefore, the product composition.³ Quasielastic neutron scattering spectroscopy (QENS) is a technique that allows for the observation of rotational and translational motions of adsorbed molecules as long as they fall within the time scales of the QENS spectrometers.⁴ The QENS technique is well placed to gain an understanding of how this diffusion changes with temperature and zeolite properties.^{4–8} Classical molecular dynamics

simulations have often been used in conjunction with QENS experiments as the time scales of the two techniques are well-matched. The combination of the molecular dynamics (MD) and QENS has proven to be important for understanding molecular motion and confined diffusion.

Methanol diffusion in acidic zeolites has been studied using QENS, although the high activity of ZSM-5 type zeolites has made the observation of methanol motion within them challenging. O'Malley *et al.*⁹ determined the self-diffusivity of methanol in zeolite Y; however, the application of similar methods to study the ZSM-5/methanol interaction revealed low methanol mobility that was largely limited to rotational motion.^{10,11} Methanol motions were limited to isotropic rotations of the methyl group or diffusion within confined spheres the size of a single zeolite pore owing to the adsorption of the methanol on the Brønsted sites, with the longer-range movements responsible for the diffusion of the methanol into and out of the pores occurring on time scales too long to be resolved by the instrument utilised.^{10,11} A more recent study has established that the Si:Al ratio of the zeolite determines the fraction of adsorbed methanol that is free to undergo these confined motions, but does not meaningfully affect the length scale of the confinement.¹²

Studying how diffusion is affected in deactivated (coked) catalysts is important in understanding the mechanism of deactivation and how coke can affect both the diffusion of reactants and products through the catalyst as it ages. Deactivation has been studied on two other catalytic systems with varying levels of success. Davidson *et al.*¹³ used QENS to study hydrogen diffusion on an unpromoted iron-based Fischer–Tropsch synthesis catalyst with various levels of hydrocarbonaceous material present within the catalyst matrix. The retained hydrocarbonaceous material complicated the analysis, with the probe hydrogen motion being difficult to distinguish from the motion of the hydrocarbonaceous material present in the catalyst.¹³ A different study by Silverwood *et al.*¹⁴ showed that QENS can be successfully used to study the methane motions inside the Mo/ZSM-5 catalyst used for the methane dehydroaromatization reaction. The coke present after one hour of reaction (2 wt. %) did not show any effect on methane diffusion, which suggests that the coke deposition at that stage in the reaction does not restrict access to the pore network.¹⁴

A report studying the effect of the retained hydrocarbons on the methanol diffusion using QENS has been published by Matam *et al.*¹⁰ In this QENS study, methanol was used as the probe molecule on a blank ZSM-5 catalyst, an MTH reacted catalyst at 350 °C, and one reacted at 400 °C. The study showed that the methanol is immobile in both the clean zeolite and the zeolite sample reacted at 350 °C. The methanol showed isotropic rotation within the zeolite pore when introduced in the MTH sample reacted at 400 °C. The increased reaction temperature induced some mesoporosity in the zeolite, which caused the methanol rotational movement to be visible within the QENS time frame. The immobility of the methanol was attributed to being either due to low mobility or due to a strong methanol interaction with the hydrocarbons already present. This issue could be potentially overcome by the use of a probe molecule of similar size to methanol but without the reactive OH group. Methane is an obvious candidate.

Li *et al.*¹⁵ reported a molecular dynamics study using methane as the diffusion probe through ZSM-5 with varying levels of coke

present. The coke was simulated by having two different models for coke deposition: a uniform deposition, which is what has been assumed happens at the early stages of the reaction, and an uneven deposition when larger amounts of coke are present. It was found from these MD calculations that a uniform deposition of coke had little to no effect on methane diffusion, but when coke is randomly distributed, the methane self-diffusion coefficient dropped. The calculated self-diffusion coefficients of methane were in the $10^{-9} \text{ m}^2 \text{ s}^{-1}$ regime, which suggests that methane diffusion will be visible within the accessible QENS time scales of our instrumentation.

This paper will focus initially on understanding the motions of methane in an activated but unreacted (fresh) ZSM-5 catalyst (ZSM5-FR) using QENS, complemented by molecular dynamic calculations. QENS analysis is then undertaken on methane in ZSM-5 catalysts under MTH reaction conditions for two different times-on-stream. A reaction time of 2 h corresponds to a catalyst conditioning stage, while a 110 h reaction time represents the catalyst after an extended period of time-on-stream. Hereafter, these samples will be referred to as MTH-2 h and MTH-110 h.

II. EXPERIMENTAL

The empty ZSM-5 catalyst was calcined under static air at 500 °C for 12 h and then dried under He flow before being loaded into aluminum annular QENS cans with a 1 mm free space. The QENS sample cans are equipped with gas handling capabilities. The MTH reacted samples were created using the Glasgow/ISIS Rig located at ISIS.¹⁶ The reaction was monitored by online mass spectroscopy, and the liquid products were collected via a catch-pot and analyzed by gas chromatography-mass spectrometry (GC-MS) using an Agilent 7890A gas chromatograph equipped with a series 5975 mass-selective detector. Component separation was achieved using a 60 m DB-1ms nonpolar capillary column, which achieved good separation of all product peaks. Detailed experimental and sample analysis has been reported elsewhere.¹⁷ Surface area analysis used a Quantachrome Quadrasorb EVO/Si with nitrogen as the probe molecule. Coke content was determined by use of thermogravimetric analysis (TGA) to remove the coke through oxidation. This was carried out under air at a temperature ramp of $10^\circ \text{C min}^{-1}$ to 900 °C, and the resulting coke %wt. values used to estimate the mass of the ZSM-5 component in each QENS sample and, hence, the number of moles of zeolite. The samples were loaded by connecting them to a known volume filled with 870 mbar of methane while holding at 373 K and the system allowed to equilibrate. The number of molecules in the sample at saturation was calculated from the resulting pressure drop and the excess methane outside the sample removed to prevent additional condensation into the sample at lower temperatures. QENS measurements took place in the IRIS spectrometer.¹⁸ Long scans of 600 μA were completed at base temperature (5 K), 225, 275, 325, and 373 K with elastic window scan measurements of 30 μA between measurements in steps of 25 K. The highest data point was limited to 373 K by the maximum temperature rating of the indium wire gaskets used to seal the cell. The QENS measurements were carried out on both the blank sample (ZSM5-FR) and then after CH_4 loading. Table I summarizes the physical characteristics of the samples measured.

TABLE I. Sample details.

	ZSM5-FR	MTH-2 h	MTH-110 h
Reaction time (h)	0	2	110
Coke (wt. %)	0	2.58	14.20
S_{BET} ($\text{m}^2 \text{g}^{-1}$)	370	397	46
$V_{\text{micropore}}$ ($\text{cm}^3 \text{g}^{-1}$)	0.16	0.15	0.01
Mass ZSM-5 (estimated) (g)	3.13	3.65	3.45
Methane (moles)	2.56×10^{-3}	1.66×10^{-3}	4.17×10^{-4}
Methane loading ($\text{CH}_4/\text{unit cell}$)	4.71	2.62	0.70

A. Molecular dynamics

1. Zeolite framework parameters

In order to better quantify the effect of both adsorbate loading and the framework acid sites on the diffusion of methane, simulations were performed for both H-ZSM-5 and its purely siliceous analog silicalite. The zeolite framework in all studies used the orthorhombic MFI structure with *Pnma* symmetry. The simulation box was a $2 \times 2 \times 2$ supercell with overall dimensions of $40.18 \times 39.48 \times 26.28 \text{ \AA}^3$ containing 2304 framework atoms in the silicalite structure and 2328 atoms in the ZSM-5 structure due to the addition of charge-compensating protons. Periodic boundary conditions were employed to simulate a realistically sized zeolite environment without increasing computational expense. Aluminum substitutions and their associated Brønsted acid protons were included in the ZSM5 framework at a level of three acid sites per unit cell (Si:Al 31:1) to match the pre-steaming experimental catalyst as closely as possible (ZSM-5-FR, Si:Al ~ 30)¹⁹ without the complication of fractional numbers of acid sites. These were distributed to maximize acid site separation in accordance with Dempsey's rule, and the Brønsted groups positioned to point into the pore channels.²⁰

The zeolite model in both cases used a flexible framework with potentials taken from work by Jackson and Catlow²¹ and expanded on by Schröder *et al.*²² based on fitting properties of α -quartz and alumina with the properties of the hydroxyl groups modified based on *ab initio* simulations. These potentials are well established, have been found to accurately describe the properties of both zeolites and SiO_2 structures,²¹ and have been used to accurately describe the behavior of small adsorbed molecules within zeolite frameworks.^{23–25} Full ionic charges were assigned to the framework T-atoms and non-hydroxyl oxygens, while partial charges were assigned to the atoms of the hydroxyl groups (designated O_b and H_b) as per Schröder *et al.*²² The long-range Coulombic interactions were evaluated via the Ewald method.²⁶ Short range pair interactions were described by a Buckingham potential for the Si–O, Al–O and O–O pairs and a Morse potential for the O_b – H_b bond; the interactions between T-atoms are regarded as having a negligible contribution and were discarded. All pair interactions were calculated with a cut-off radius of 10 \AA . A harmonic three-body potential was used to describe and accurately constrain the geometry of the O–Si–O and O–Al–O triads. The values of the parameters for these potentials are given in Table II.

2. Methane parameters

The properties of the methane carbons and hydrogens and the intermolecular interactions between adsorbate molecules were parameterized using OPLS_2005, a generalized all-atom force field for the simulation of organic molecules.²⁷ These parameters are derived from both experimental data and quantum chemical simulations and can predict small molecule behavior in both gas and

TABLE II. Potential parameters for intramolecular zeolite interactions. H_b and O_b represent the Brønsted acid proton and its associated bridging oxygen, respectively.

Atomic charges			
Atom	Charge (a.u.)		
Si	+4.000		
Al	+3.000		
O	−2.000		
O _b	−1.426		
H _b	+0.426		
Buckingham potentials			
Atoms	<i>A</i> (eV)	<i>ρ</i> (Å)	<i>C</i> (eV Å ⁶)
O–O/O _b	22 764.0	0.149 00	27.8800
Si–O	1 283.91	0.320 52	10.6616
Si–O _b	983.557	0.320 52	10.6616
Al–O	1 460.30	0.299 12	0.0
Al–O _b	1 142.68	0.299 12	0.0
O–H _b	311.970	0.250 00	0.0
Morse potentials			
Atoms	<i>E</i> ₀ (eV)	<i>r</i> ₀ (Å)	<i>k</i> (Å ^{−1})
O _b –H _b	7.0525	0.9485	2.1986
Three-body potentials			
Atoms	<i>k</i> (eV rad ^{−2})	ϑ ₀ (deg)	
O–Si–O/O _b	2.097 24	109.470	
O–Al–O/O _b	2.097 24	109.470	

condensed phases across a wide range of temperatures with good accuracy. In this implementation of methane, all hydrogens are assigned a charge of +0.06 atomic units, and the carbon charge set at -0.24 a.u. to neutralize the overall molecular charge. C-H bonds and H-C-H bond angles are described by harmonic potentials and the intermolecular pair interactions as Lennard-Jones potentials. All parameters are given in Table III.

3. Zeolite-methane interaction parameter

The framework-adsorbate interactions were taken from the work of Kiselev *et al.*²⁸ on deriving potential energies of interaction from atom electronic properties as implemented for hydrocarbons in zeolites by Vetrivel *et al.*,²⁹ Catlow *et al.*,³⁰ and O'Malley *et al.*⁹ All interactions were modeled as Lennard-Jones potentials using the parameters in Table IV; interactions involving the framework T-atoms were once again discounted as negligible.

4. Simulation procedure

All simulations were performed using the DL_POLY 4 code,³¹ the DL_FIELD package was used to assist in the preparation of the necessary input files,³² and analysis of the resulting simulations was assisted by use of the MDANSE software package.³³ For the initial configuration, the methane molecules were placed in the center of the zeolite pore channels equidistantly throughout the zeolite supercell. Loadings of 4 and 9 methane molecules per unit cell in both the

TABLE III. Potential parameters for intramolecular and intermolecular methane-methane interactions.

Intramolecular interactions		
Atomic charges		
Atom	Charge (a.u.)	
C	−0.24	
H	+0.06	
Harmonic bond potentials		
Atoms	k (eV rad ^{−2})	r_0 (Å)
C–H	29.4876	1.090 00
Harmonic angle potentials		
Angle	k (eV rad ^{−2})	ϑ_0 (deg)
H–C–H	2.862 03	109.500
Intermolecular interactions		
Lennard-Jones pair potentials		
Atoms	ε (eV)	σ (Å)
C–C	$2.862\,03 \times 10^{-3}$	3.500
C–H	$1.929\,58 \times 10^{-3}$	2.958
H–H	$1.300\,92 \times 10^{-3}$	2.500

TABLE IV. Intramolecular potentials describing methane-framework interactions.

Lennard-Jones pair potentials		
Atoms	ϵ (eV)	σ (Å)
O-C	7.083×10^{-3}	2.923
O _b -C	8.280×10^{-3}	3.150
O/O _b -H	4.987×10^{-3}	2.557
H _b -C	2.990×10^{-3}	2.806
H _b -H	8.510×10^{-4}	1.784

ZSM-5 and silicalite frameworks were chosen to match the experimental loading value for the fresh catalyst (ZSM5-FR) and to observe the effect of methane loading on diffusion.

All simulations were performed in the canonical (NVT) ensemble using a Nosé-Hoover thermostat with a 1 ps thermal exchange time constant to maintain the desired temperature for each simulation.³⁴ The simulation time step was 0.5 fs throughout. All systems were initially equilibrated for 1 ns at 270 K in order to ensure that low-temperature simulations began from a stable distribution of the methane molecules within the zeolite. They were then equilibrated for a further 1 ns at the target temperature for the simulation followed by a production run of 5 ns, chosen as being sufficient to achieve true diffusive motion for the adsorbed methane. The atomic coordinates and velocities for the system were saved every 2000 steps (1 ps) for analysis.

MD simulations were performed on both silicalite and ZSM-5 type frameworks using the molecular force-field and simulation procedure given above. Loading levels of 4 and 9 methane molecules per unit cell were simulated in order to determine the effect of loading level on the diffusion properties. Simulations were performed at 95, 130, 170, 225, 270, 325, and 375 K so as to match the range of temperatures investigated by detailed QENS analysis and to provide information on the low temperature behavior of the simulated systems. 95 K was chosen as being immediately above the melting point of solid methane and therefore the first temperature where mobility is likely to be observed.

III. RESULTS

A. Elastic window scan analysis

The initial examination of the mobility of the system was through an Elastic Fixed Window Scan (EFWS) analysis because of its ease of calculation and ability to provide an overview of the changes in diffusion behavior with temperature across the full range studied.

1. QENS results

The EFWS of methane in ZSM5-FR shows the expected behavior of increased mobility with temperature, with the greatest increase in mobility occurring at low temperatures (Fig. 1). A small inflection in the slope of the EFWS trace occurs between 75 and 100 K due to the methane passing through its melting and boiling points,

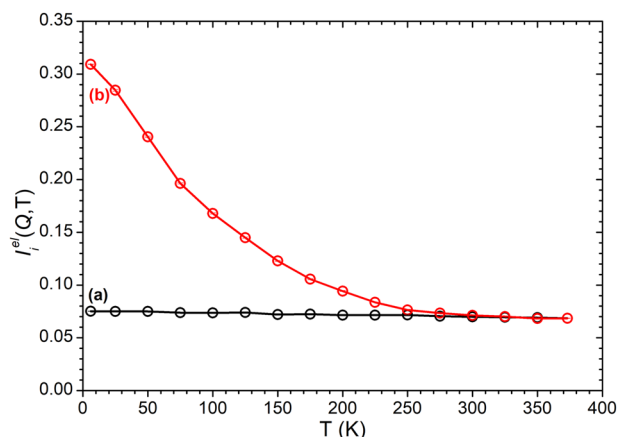


FIG. 1. Experimental elastic intensity vs temperature for unloaded ZSM5-FR (a) and methane in ZSM5-FR at a calculated loading of 4.70 molecules per unit cell (b).

respectively. One notable feature is that at temperatures of 300 K and above, the elastic intensity in the loaded sample is essentially identical to that recorded for the unloaded ZSM5-FR prior to hydrocarbon loading. This shows that at these temperatures, the methane is fully mobile and does not contribute to the measured elastic intensity at all, with the remaining EFWS intensity values being entirely due to scattering from the zeolite framework. The methane still contributes to the quasielastic scattering and may be analyzed through fitting; however, such high levels of mobility are likely to complicate this process.

2. MD results

It is possible to calculate the $S(Q, \omega)$ scattering function of a system simulated using MD by using the atomic positions in the molecular trajectory file and the Van Hove self-correlation function.³⁵ These simulated $S(Q, \omega)$ functions can then be used to derive a simulated EFWS plot across the temperature range simulated. Scattering functions were simulated in the range $0.1 \leq Q \leq 5 \text{ \AA}^{-1}$ at 0.1 \AA^{-1} intervals, but the integrated intensities used to calculate the theoretical relative elastic intensity were limited to the momentum transfer values that are accessible on the IRIS spectrometer ($0.42\text{--}1.85 \text{ \AA}^{-1}$, simulation integration performed from 0.4 to 1.9 \AA^{-1}).¹⁸

The resulting simulated EFWS for simulations in H-ZSM-5 (Fig. 2) conforms closely to the experimental data in the blank ZSM-5 at temperatures above 200 K, which includes one point (225 K) where the experimental spectrum still possesses some methane-derived elastic intensity. The overall trend is toward a plateau value at $\sim 10\%$ of the initial relative intensity. This confirms that all methane molecules are fully mobile by $\sim 300\text{--}350 \text{ K}$, and the remaining elastic intensity is due to scattering from the essentially immobile zeolite framework. That the final relative intensity values in the simulated spectra being at a slightly lower level than in the experimental case can be attributed to the absence of any background intensity in the simulations and that the simulated results can observe all motions that occur during the simulation,

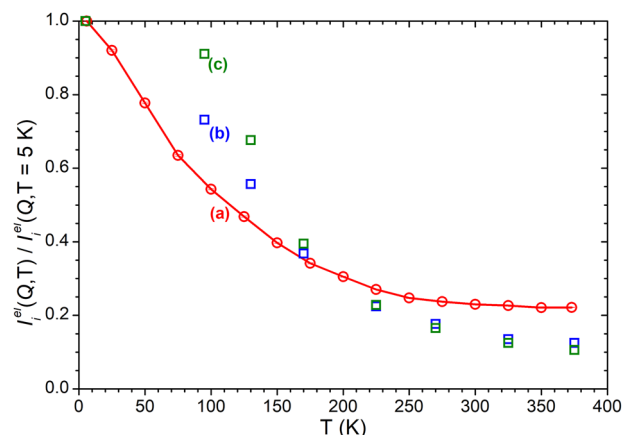


FIG. 2. Comparison of the experimental EFWS of CH₄ in ZSM5-FR (a) with simulated relative elastic intensities for methane in H-ZSM-5 (b) and silicalite (c) derived from molecular dynamics calculations. All values normalized against elastic intensity at $T = 5 \text{ K}$.

not just those that occur within the time window accessible on the spectrometer used.

An anomaly in the simulated data is observed in the simulations performed at 95, 130, and 170 K, where the MD simulation persistently underestimates the level of mobility in the sample at these temperatures. Surprisingly, this effect is even more heavily pronounced in the simulation of methane movement in the pure SiO₂ framework [Fig. 2(c)]. This suggests that the problem may be due to an overestimation of the intermolecular forces between the methane molecules in the simulation force-field. The decreased magnitude of the effect in the H-ZSM-5 simulation would then be attributable to the acid site-methane bonding disrupting the structure of the solid methane and decreasing the energy required for methane molecules to break free into the gas phase. Indeed, this critical matter concerning the suitability of the selected force-field constitutes “work in progress.”

An alternative explanation is provided by observations made in a molecular dynamics study by López *et al.*³⁶ of a change in the preferred low-energy site of methane in silicalite structures, which occurs at 250 K. Below this temperature, the methane prefers locations within the straight channels, while above it the lowest energy site lies in the channel intersections, with a corresponding change in the energy barriers to diffusion. While this is a possible explanation for the observed behavior, the López investigation was carried out at infinite dilution and caution should be used in extrapolating from such studies to systems where methane-methane interactions are significant.³⁷ Therefore, the source of the discrepancy cannot be assigned with certainty at this time.

B. Diffusional behavior

Figure 2 shows the region from 200 to 375 K to exhibit good agreement between experimental results and simulation, with four temperatures where high resolution QENS spectra are available for analysis. The results obtained by both methods will be compared in this section.

1. QENS results

The data were fit using a broadened delta function for the instrument resolution, one Lorentzian peak to model the quasi-elastic broadening and a linear background function. The broadened delta used is the base temperature scan of the blank ZSM-5. The QENS spectra with respect to Q are complicated by the contribution of coherent Bragg scattering from the zeolite framework. However, attempting to subtract the empty zeolite from the methanol dosed sample data resulted in negative peaks, therefore the fits were made with the zeolite still present.

Four diffusion models were tested in order to fit the data. Each model describes jump-type diffusion behavior and relates the half-width at half-maximum (HWHM) of the Lorentzian broadening at a given Q value, $\Delta\omega(Q)$, to the residence time of the diffusing molecule between jumps, τ , and the length of each jump. The model of Chudley and Elliott (CE)³⁸ assumes a constant jump distance of length d , resulting in the relationship described by Eq. (1). The models of Hall and Ross (HR)³⁹ and Singwi and Sjölander (SS)⁴⁰ assume a distribution of jump lengths, of a different form in each case, and link the broadening to the mean squared jump distance, $\langle r^2 \rangle$, by the relationships in Eqs. (2) and (3), respectively. Finally, a model proposed by Jobic and Theodorou⁴ (Jobic) models differences in jump lengths by reference to terms for the average jump length, d_0 , and the degree of delocalization of the molecule between jumps, r_0 , in the relationship in Eq. (4),

$$\Delta\omega(Q) = \frac{1}{\tau} \left(1 - \frac{\sin(Qd)}{Qd} \right), \quad (1)$$

$$\Delta\omega(Q) = \frac{1}{\tau} \left[1 - \exp \left(-\frac{Q^2 \langle r^2 \rangle}{6} \right) \right], \quad (2)$$

$$\Delta\omega(Q) = \frac{1}{6\tau} \frac{Q^2 \langle r^2 \rangle}{1 + Q^2 \langle r^2 \rangle / 6}, \quad (3)$$

$$\Delta\omega(Q) = \frac{1}{\tau} - \left[\frac{\sin Qd_0}{Qd_0} \exp \left(-\frac{Q^2 \langle r_0^2 \rangle}{2} \right) \right]. \quad (4)$$

In each case, once the experimental data are fit to the models in Eqs. (1)–(4), the predicted methane self-diffusion constant (D_s) can be derived from the fitted values for (average) jump length and residence time by means of the relationship $D_s = \langle r^2 \rangle / 6\tau$. Following an Arrhenius relationship, the natural log of these diffusion coefficients can be plotted against inverse temperature. A straight line verifies that the data obey the Arrhenius relationship and enables the activation energy for the motion observed to be determined.

Figure 3 shows the Full Width Half Maximum (FWHM, Γ) derived from fitting the experimental data compared with the Γ of the four jump diffusion models. Table V shows the parameters used for each of the different models and the calculated diffusion coefficient for each one. The fit error shown in Table V is calculated from the standard deviation of the residual fits and provides an indication of goodness of fit. When trying to establish which model fits the data better, the different constraints were initially left to float. However, this resulted in the fitted values for the mean square jump distance changing without a noticeable trend. The fit was then modified to fix the $\langle r^2 \rangle$ value to that obtained by fitting at 225 K in all subsequent temperature fits. This did not seem to noticeably change the fit of the models for 225, 275, and 325 K with the $\langle r^2 \rangle$ value staying within ± 2 Å.

The 373 K datasets are difficult to fit, with the $\langle r^2 \rangle$ value for the Jobic model in particular being higher than anticipated. This

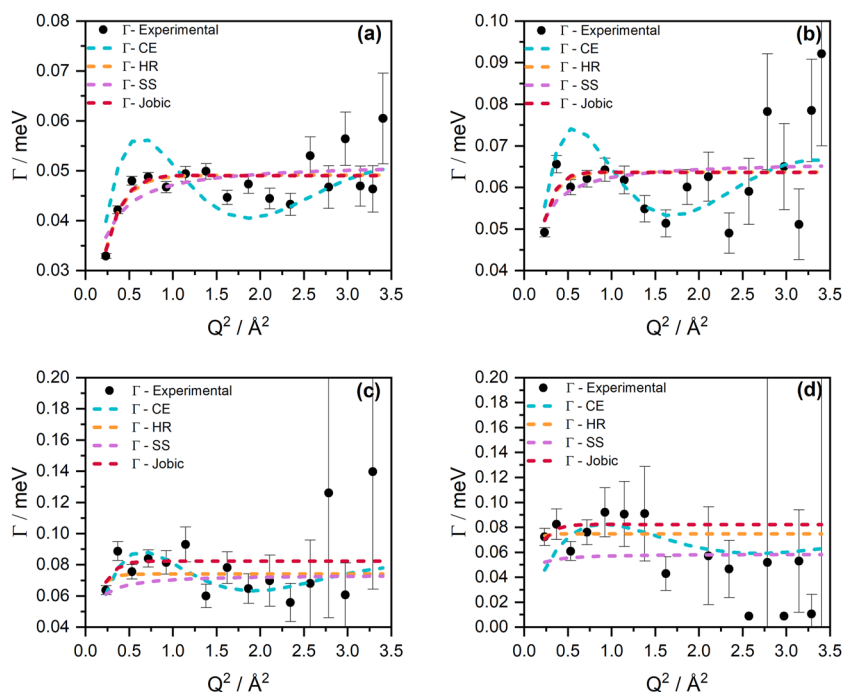


FIG. 3. HWHM (Γ) vs Q^2 for the Lorentzian fit on each temperature for the fresh ZSM-5 with methane (a) 225 K, (b) 275 K, (c) 325 K, and (d) 373 K.

TABLE V. Diffusion coefficients (D), residence times (τ), and mean square jump lengths ($\langle r^2 \rangle$), calculated using the four different jump models.

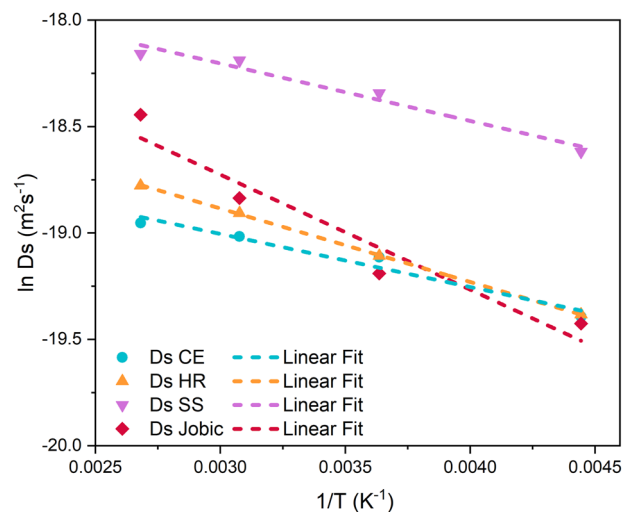
Temperature (K)	Models	Parameters		
		D ($\text{m}^2 \text{s}^{-1}$)	τ (ps)	$\langle r^2 \rangle$ (\AA^2)
225	CE	3.78×10^{-9}	14.16	32.1
	HR	3.82×10^{-9}	13.40	30.8
	SS	8.20×10^{-9}	12.74	62.7
	Jobic	3.66×10^{-9}	13.44	29.6
275	CE	5.00×10^{-9}	10.69	32.1
	HR	5.03×10^{-9}	10.20	30.8
	SS	1.08×10^{-8}	9.68	62.7
	Jobic	4.63×10^{-9}	10.64	29.6
325	CE	5.51×10^{-9}	9.11	32.1
	HR	6.15×10^{-9}	8.70	32.1
	SS	1.26×10^{-8}	8.27	62.7
	Jobic	6.60×10^{-9}	8.00	31.7
373	CE	5.87×10^{-9}	9.70	32.1
	HR	7.00×10^{-9}	8.50	35.7
	SS	1.30×10^{-8}	8.06	62.7
	Jobic	9.76×10^{-9}	7.00	40.9

could be due to the mobility of the methane becoming so fast that the data are too noisy for a proper fit. From Fig. 3, it is apparent that the models seem to have a better fit at low Q values ($Q^2 \leq 1.5$), with the fit deviating at higher Q values. Literature values for the diffusion coefficient of methane in NaZSM-5 at 200 and 250 K are 2.7×10^{-9} and $5.5 \times 10^{-9} \text{ m}^2 \text{s}^{-1}$, respectively.⁴¹ These literature values in Na-ZSM-5 match those calculated here via the Chudley–Elliot, Hall–Ross, and Jobic models; the diffusion constant calculated by the Singwi–Sjölander model shows a higher diffusion coefficient than anticipated from the literature data (Table V).

The Arrhenius relationship between the natural logarithm of the diffusion coefficients and the inverse of temperature is plotted in Fig. 4. Table VI shows the derived activation energies of the motions that the different jump diffusion models are describing. The Jobic model is seen to be the closest fit when comparing the activation energies with the literature value for CH_4 in ZSM-5, which were recorded with a different Si/Al of ZSM-5 and a different cation present (Na). The difference in Si/Al ratio of a zeolite, as well as the presence of a different cation, could potentially change the activation energy of the methane motions within the zeolite. Indeed, Perez-Carbajo and co-workers have calculated the dependence of CH_4 and CO_2 diffusion within Na and Ca promoted zeolite MFI by varying the Al mole fraction and its distribution within the porous network.⁴²

2. Molecular dynamic calculations

Accurate calculation of diffusion constants from the statistics of molecular dynamics simulations requires simulation lengths long enough that the system achieves true diffusive motion and the mean

**FIG. 4.** Arrhenius plot of the natural log of the diffusion coefficient over the inverse of temperature for the ZSM-5 with methane.

squared displacement (MSD) of the adsorbed molecules becomes linear with respect to time. As shown in Fig. 5, the systems studied here achieve this for the majority of the simulation runtime. The fluctuations at longer time values observed for the higher temperature simulations are because the MSD is calculated as an ensemble average over all possible molecules and origins, with each time step in the simulation being treated as a “time zero” for a displacement trajectory. As the length of the time window being considered approaches the full length of the simulation, the number of potential origins for averaging is reduced, resulting in less consistent results. By limiting the analysis to the linear portion of the MSD trace, the self-diffusion constants at each temperature may be calculated using the Einstein relationship

$$D_s = \frac{1}{6} \lim_{t \rightarrow \infty} \frac{d}{dt} \langle (r_t - r_0)^2 \rangle, \quad (5)$$

where the term in braces represents the MSD.

The calculated MSD values are given in Table VII: these values show a disconnect between the diffusion constants at low temperatures and those from simulations performed above 200 K. This is consistent with the results observed in the elastic window scan data (Fig. 2), and the same explanation proposed there applies.

TABLE VI. Table of activation energies calculated from Fig. 4.

Jump diffusion models	Activation energy (kJ mol^{-1})
Chudley–Elliot	2.07
Hall–Ross	2.86
Singwi–Sjölander	2.24
Jobic	4.49
Literature– CH_4 in silicalite ³⁴	4.3 ± 1
Literature– CH_4 in Na-ZSM-5 ³³	4.7 ± 0.7

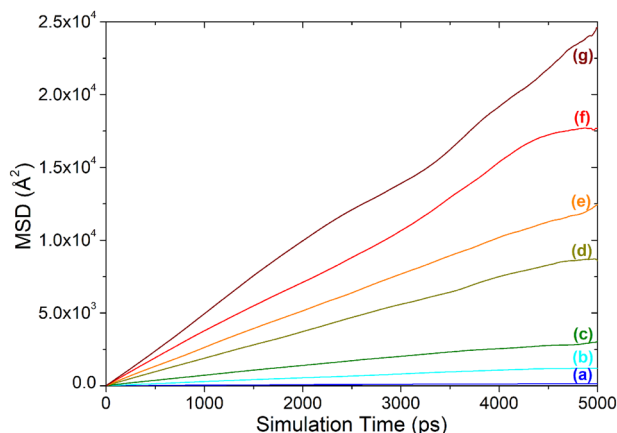


FIG. 5. Mean squared displacement vs time for methane in H-ZSM-5 at a loading of 4 molecules per unit cell, calculated at simulation temperatures of 95 K (a), 130 K (b), 170 K (c), 225 K (d), 270 K (e), 325 K (f), and 375 K (g).

Comparison of the results above 200 K, which are more in line with experimental observations, shows that the difference in diffusion constants between silicalite and H-ZSM-5 structures is quite small in both the 4- and 9-molecule per unit cell cases. In both structures, the difference between the low and high loaded simulations in the same material is more significant. This suggests that the higher loaded simulation in both cases is sufficiently congested that methane–methane interactions are the limiting factor in determining the bulk diffusion through the zeolite pores, with the effect of methane–zeolite interactions being masked by this pore congestion effect. In the 4 CH₄ molecules/u.c. simulations, where differences exist, the methane diffuses slower in H-ZSM-5 compared to silicalite as would be expected due to the additional Brønsted OH-adsorbate interactions. The activation energies similarly show

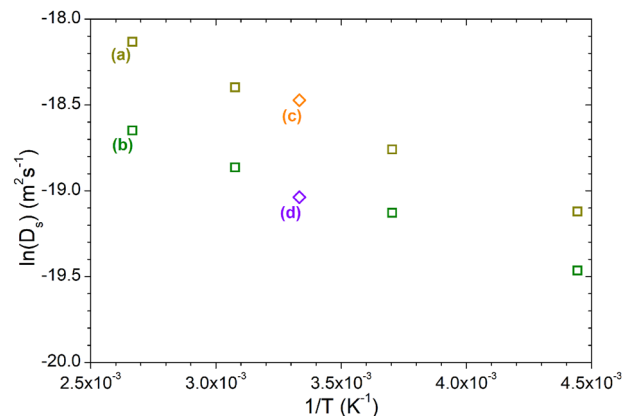


FIG. 6. Arrhenius plot comparison of diffusion in silicalite calculated by MD at 4 (a) and 9 (b) molecules per unit cell; literature values for diffusion in silicalite at 4 (c) and 8 (d) molecules per unit cell as reported by Leroy *et al.*⁴⁴

the expected trend, with the value in H-ZSM-5 being 110% of that in silicalite. This compares favorably with the E_a of 4.84 kJ/mol determined experimentally by QENS (Table VII) being 105% of that reported for methane in silicalite by Caro *et al.*⁴³ This suggests that the molecular dynamics force field is accurately describing the effect of the Brønsted acid sites on the overall behavior of the system.

The molecular dynamics results obtained are consistent with those found in the literature for comparable systems. As shown in Fig. 6, the simulations in silicalite closely match those reported by Leroy *et al.*⁴⁴ for comparable loadings at 300 K. It is notable that Leroy *et al.* reported that its molecular dynamics simulations produce diffusion constants ~2–2.5 times larger than those of QENS investigations of methane in silicalite by Jobic and co-workers. Unfortunately, we were unable to obtain the exact values of these

TABLE VII. Self-diffusion coefficients (D_s) and activation energies (E_a) for methane in silicalite and H-ZSM-5 calculated from MD results. Calculated MD:QENS ratios are for H-ZSM-5 simulations.

T (K)	D_s (m ² s ⁻¹)				Ratio MD:QENS	
	Silicalite		H-ZSM-5			
	4 × CH ₄ per u.c.	9 × CH ₄ per u.c.	4 × CH ₄ per u.c.	9 × CH ₄ per u.c.	4 × CH ₄ per u.c.	9 × CH ₄ per u.c.
95	8.22×10^{-11}	5.57×10^{-11}	4.00×10^{-11}	5.64×10^{-11}
130	4.93×10^{-10}	3.87×10^{-10}	4.00×10^{-10}	4.52×10^{-10}
170	1.99×10^{-9}	1.50×10^{-9}	1.81×10^{-9}	1.10×10^{-9}
225	4.97×10^{-9}	3.51×10^{-9}	4.06×10^{-9}	3.10×10^{-9}	1.11:1	0.85:1
275	7.13×10^{-9}	4.93×10^{-9}	5.73×10^{-9}	4.25×10^{-9}	1.24:1	0.92:1
325	1.02×10^{-8}	6.43×10^{-9}	8.79×10^{-9}	6.18×10^{-9}	1.33:1	0.94:1
375	1.34×10^{-8}	7.96×10^{-9}	1.23×10^{-8}	7.95×10^{-9}	1.27:1	0.81:1
D_0 (m ² s ⁻¹)	5.15×10^{-8}	3.19×10^{-8}	5.38×10^{-8}	4.04×10^{-8}
E_a (kJ mol ⁻¹)	4.39	4.26	4.84	5.01	1.08:1	1.12:1

QENS investigations to allow a direct comparison to our own QENS and MD figures due to the studies by Jobic only giving the methane D_s values in graphical form.

In our own experiments, discounting the simulations below 200 K and comparing the values derived at higher temperatures with the QENS results show that the simulated and experimental data are in broad agreement. For the 4 molecules per unit cell in ZSM-5 simulation, which is the closest match to the experimental data in terms of methane loading, the calculated diffusion constants (Table VII) match those recorded experimentally (Table VI) to within 35%, which is typical for MD simulations at this level of simulation accuracy.²⁵ The simulated D_s values are higher than those obtained experimentally as shown in Table VII and Fig. 7. This is because molecular dynamics predictions assume a perfect crystal structure, which does not account for the presence of local defects, silanol sites, crystal edge effects, or inhomogeneous Brønsted site locations; all of which will tend to reduce the experimentally observed diffusion values.

C. Diffusional behavior of hydrocarbon coke in coked samples

Characterization of the coked samples is reported elsewhere.¹⁷ The samples were reacted at 350 °C under methanol-to-hydrocarbon conditions and reproduce expected MTH trends.¹⁷ The coked samples were measured by QENS first without methane and then after methane dosing. However, the coke within the samples caused complications in analyzing the QENS spectra. Replicating trends reported by Davidson *et al.* on a different catalytic system,¹³ the coke contains hydrogen atoms that are mobile. Attempts to subtract the non-methane dosed QENS spectra from the methane dosed spectra were unsuccessful, as negative peaks appeared. Therefore, as above, all fits were attempted without subtracting the zeolite contribution. Due to the degree of coking, and the fact that the samples were flushed before the QENS measurement, it is assumed that all volatile hydrocarbon species have been removed and that the coke present would contain only localized

motions. The localized motion models considered can be found in the [supplementary material](#) to this paper. The fitting of the experimental data has been done without adding any constraints to the models. The r values were left to float to find the best fit possible.

Both coked samples were fitted using the same combination of a broadened delta peak, single Lorentzian, and linear background used to model the data in ZSM5-FR above. The resolution file used for creating the broadened delta was the MTH-2 h/MTH-110 h scan at base temperature used for each coked sample. From those fits, the elastic incoherent structure factor (EISF) values were extracted, this being the fraction of the total scattering intensity that is elastic at each value of Q . These show a decrease with increasing Q , which is indicative of constrained rotational motion. The EISF models as a function of Q can be found in Figs. S2 and S3 of the [supplementary material](#). Owing to the variety of hydrocarbons present, especially for the MTH-2 h sample, where no assignment could be made of the INS spectra,¹⁷ the r -values were left to float. This should allow the r -value to settle to a number that would closely represent the average rotational distance.

The r -values for the model of rotation could be due to the whole molecule rotating or because part of the molecule is rotating. Since any weakly adsorbed molecules likely to be capable of full rotation were removed by flushing prior to the QENS measurements, partial rotation is more likely.

Table VIII shows the fitting parameters for the MTH-2 h sample. The r -values obtained for isotropic rotations, both spherical and planar, lie between 1.6–2.1 Å. The values are too small for this to be due to a free benzene ring motion that has an r -value of ~2.5–3 Å.^{45,46} Therefore, free isotropic rotation of methylated aromatic coke species is unlikely. Translation in a sphere could also be a possibility with a reduced pore size of 3 Å, assuming the molecule that is moving is small enough to be able to do so. The percentage of the hydrogen atoms in the sample, which remains immobile, shown as P_i in Table VIII, is high for all the rotational models considered, which fits with the expectation of the hydrocarbons of the residual hydrocarbon pool being adsorbed to the zeolite surface. However, it must be noted that fitting the QENS data also required a

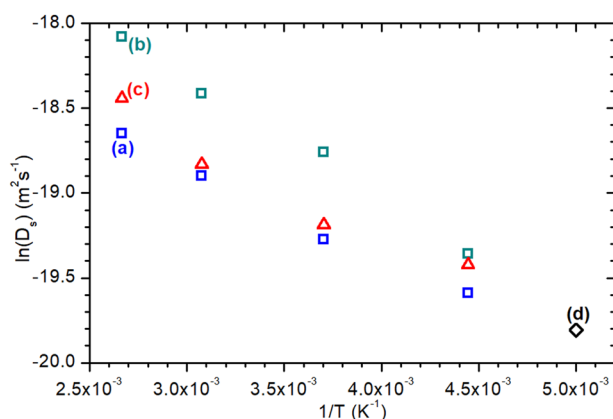


FIG. 7. Arrhenius plot comparison of CH_4 diffusion in H-ZSM-5 calculated by MD at 4 molecules per unit cell (a) and 9 molecules per unit cell (b); experimental QENS values at 4.70 mol/u.c. in ZSM5-FR as determined above (c); and the experimental QENS value at 4 mol/u.c. in Na-ZSM-5 as reported by Jobic *et al.*⁴¹ (d).

TABLE VIII. Fitting parameters for rotational fitting models for MTH-2 h.

Rotational fitting models		QENS temperatures			
		225 K	275 K	325 K	373 K
Isotropic planar rotation	r (Å)	1.99	1.99	1.61	1.60
	P_i (%)	94	92	84	81
Isotropic rotation spherical	r (Å)	1.80	1.92	2.07	2.05
	P_i (%)	91	91	82	81
2-site rotation	r (Å)	2.70	2.86	3.00	3.00
	P_i (%)	87	85	73	67
3-site rotation	r (Å)	1.70	1.65	1.73	1.73
	P_i (%)	90	89	78	76
Translation in a sphere	r (Å)	3.08	3.00	2.74	2.75
	P_i (%)	94	92	84	81

background. Background intensity is usually related to fast motions, faster than the instrument is able to detect, which broaden out the QENS peak to the baseline, but the origins of such movement are unknown.

The model fit parameters for sample MTH-110 h are presented in Table IX. The immobile fraction is also large for all models, but the immobile fraction does not decrease with temperature, as was observed in the MTH-2 h sample. This could suggest that the immobile hydrogen atoms are hydrogen atoms at the edges of large polycyclic aromatic molecules or the amorphous coke, which would be expected to be immobile. This is consistent with what is known of the amorphous coke present within a zeolite coked to such an extent.¹⁵

All the models seen in Fig. S3 of the supplementary material seem to fit the data well, especially at low temperatures. The translation in the sphere fails at higher temperatures: the fit cannot match the experimental data, even with no constraints. This is to be expected, as the motions observed are most likely due to anchored hydrogens. Isotropic rotations show a good fit at all temperatures, and the r -values are too small for benzene, methylated benzenes, or polycyclic rotation (molecules associated with the hydrocarbon pool). The r -value of the three site jump rotation ranges from 1.28 to 1.54 Å; this is closest to a hydrogen three jump in an anchored methyl atom that is 1.48 Å.⁹ The r -values for that need to be adjusted slightly, but the shape of the curve should remain the same. If that is the case, then the EISF could possibly be observing methyl rotation of the methyl groups attached to the methylated aromatics stuck within the zeolite pores.

D. Diffusional behavior of methane in coked samples

The fitting of the QENS data was carried out as described above. The loaded samples, in theory, should have at least two motions associated with them. These are the rotational movement of the coke, described above, and the movement of the methane. However, the best fit of the data was again achieved with a broadened delta resolution function using the base temperature scan of the

MTH-2 h/MTH-110 h sample with no methane for the instrumental resolution, one Lorentzian and one background. The fit of a single Lorentzian is surprising, as movement of the coke was observed in the empty samples. However, the Lorentzian in this case has different fitting parameters than the empty coked samples. The parameters of the Lorentzian match loosely with those expected for translational diffusion of methane for the methane in the MTH-2 h sample (see Fig. S4 of the supplementary material). For the methane in the MTH-110 h, the fitting parameters are still associated with rotational movement, with the r -values restricted to motions associated with methane rotations (see Fig. S6 of the supplementary material).

The methane present within the MTH-2 h sample is seen to fit better a translational diffusion model. The best fit model again is the Jobic model as was seen in the fresh ZSM-5. The activation energy for the methane motion is 3.55 kJ mol⁻¹, which is surprisingly lower than the derived activation energy of the fresh sample (4.49 kJ mol⁻¹). From Li *et al.*,¹⁵ it has been discussed that at early stages, the diffusion of methane is undisturbed by the coke. The simulations of methane loaded in silicalite has shown that methane-methane interactions can play an important role in the methane motion. It could therefore be that the lower loading of methane in the coked sample is causing the activation energy barrier to decrease.

For the MTH-110 h methane loaded sample, none of the translational diffusion jump models fit the experimental data. The experimental EISF matches more closely to the translation in a sphere model, where the methane is undergoing small translational motions within a confined sphere with a radius of 2 Å and an immobility percentage of 79%–89%. However, at the two higher temperatures, it is unclear if the motion observed is due to the coke or to the methane.

IV. CONCLUSIONS

The diffusion of methane through fresh ZSM-5 and ZSM-5 that has been through an MTH reaction at different times on stream (2 and 110 h) has been studied. Previous studies using methanol as the probe have shown that the methanol–Bronsted acid sites interactions were dominant even in coked catalysts.⁹ In contrast, with methane as the probe molecule, the degree of mobility is much higher, which results in complications due to the methane motions becoming too fast to be observed at temperatures above 250 K for the fresh and early stage MTH reacted sample and above 200 K for more heavily coked materials.

Methane within an unreacted ZSM-5 shows diffusion constants and activation energies closely matching those previously observed for methane in different Si:Al ratio ZSM-5's; the Jobic model of jump diffusion provides the best fit for its motion within the zeolite pore network (Table V). The diffusion of methane in ZSM5-FR and silicalite has been simulated by molecular dynamics at two different levels of loading and compared with the results from experimental QENS observations. The diffusion constants calculated from MD simulations above 200 K closely match those reported in the literature for similar systems.⁴⁴ They produce estimates of mobility that closely match those obtained by experiment (Table VII), confirming that the molecular force field used in these simulations can accurately describe small C₁ molecules as well as the larger alkanes and olefins whose simulations are reported above. The force field's

TABLE IX. Fitting parameters for rotational fitting models for MTH-110 h.

Rotational fitting models		QENS temperatures			
		225 K	275 K	325 K	373 K
Isotropic planar rotation	r (Å)	1.20	1.20	1.30	1.28
	P_i (%)	90	89	89	89
Isotropic rotation spherical	r (Å)	1.48	1.48	1.60	1.48
	P_i (%)	90	89	89	89
2-site rotation	r (Å)	2.20	2.21	2.67	2.36
	P_i (%)	83	82	84	83
3-site rotation	r (Å)	1.30	1.28	1.54	1.37
	P_i (%)	88	87	87	87
Translation in a sphere	r (Å)	1.80	1.82	1.91	1.90
	P_i (%)	90	88	87	87

ability to describe the behavior of methane in the liquid phase is less accurate, owing to the way in which the intermolecular hydrocarbon parameters were derived. Comparison of the simulations in the 200–375 K region shows that methane–zeolite interactions are less significant in this temperature range than methane–methane ones due to congestion of the pores. This observation is consistent with the QENS results showing that the methane is fully mobile within the zeolite at these temperatures and that no methane remains strongly adsorbed to the pore walls.

Analysis of coked zeolite samples is more complicated due to problems separating the contributions of hydrogen groups within the coke. QENS fitting shows that methane diffusion is not affected to a large degree in the early stage MTH sample (MTH-2 h), agreeing with the suggestion made in the literature that the coke present is uniform in nature.¹⁵ The slightly lower diffusion coefficients and lower activation barriers observed in the coked sample when compared with the fresh sample are attributed to the lower methane loading in the coked sample. Diffusion through the heavier coked sample is much more severely hindered, with methane motions being limited to confined translation within a sphere smaller than the pore size in ZSM-5 (2 vs 2.75 Å), indicating that coke buildup is intruding even into “unblocked” pores.

It is noted that methane loading in MTH-110 h is so low (0.7 mol_{CH₄}/mol_{ZSM-5}) that distinguishing between the methane motion and rotational contributions from the coke is challenging. Analysis of the coke QENS contributions could not assign the motion with certainty due to the complex nature of the coke composition; however, rotation of methyl groups attached to immobilized aromatics is a likely candidate.

Although methane has proven a suitably inert probe molecule for investigating C₁ mobility in zeolites, its extremely high mobility has resulted in limited ability to draw conclusions on the character of the motions at catalytically relevant temperatures. Investigating this behavior requires either higher resolution QENS instruments capable of resolving shorter time scales or the use of larger, less-mobile probes. The use of ethane ($D_s = 3 \times 10^{-9} \text{ m}^2 \text{ s}^{-1}$ at 300 K)⁴⁷ as a probe could serve for the latter approach, with the second methyl group acting as an inert replacement for the –OH group in methanol.

SUPPLEMENTARY MATERIAL

See the [supplementary material](#) for localized motion models; EISF of MTH-2 h and MTH-110 h samples; the MTH-2 h sample with methane-diffusion coefficients, residence times, and mean square jump lengths; and the MTH-110 h sample with methane-fitting parameters for rotational models and EISF experimental data fitted with rotational models.

ACKNOWLEDGMENTS

The work was funded by Johnson Matthey plc through the provision of industrial CASE studentships in partnership with the EPSRC, A.Z. (Grant No. EP/N509176/1) and A.P.H. (Grant No. EP/P510506/1). Experiments at the ISIS Neutron and Muon Source were made possible by beam time allocations from the Science and Technology Facilities Council. The resources and support provided by the UK Catalysis Hub are gratefully acknowledged.

AUTHOR DECLARATIONS

Conflict of Interest

The authors have no conflicts to disclose.

Author Contributions

Alexander P. Hawkins: Data curation (supporting); Formal analysis (lead); Investigation (supporting); Validation (supporting); Writing – original draft (lead); Writing – review & editing (supporting). **Andrea Zachariou:** Data curation (supporting); Formal analysis (supporting); Investigation (supporting); Validation (supporting); Writing – review & editing (supporting). **Ian P. Silverwood:** Formal analysis (supporting); Methodology (supporting); Validation (supporting). **Chin Yong:** Formal analysis (supporting); Methodology (supporting); Software (supporting). **Paul Collier:** Conceptualization (supporting); Funding acquisition (supporting); Project administration (supporting); Supervision (supporting). **Ilian Todorov:** Formal analysis (supporting); Methodology (supporting); Software (supporting). **Russell F. Howe:** Formal analysis (supporting); Methodology (supporting); Validation (supporting); Writing – review & editing (supporting). **Stewart F. Parker:** Formal analysis (supporting); Investigation (supporting); Methodology (supporting); Supervision (supporting); Validation (supporting); Writing – review & editing (supporting). **David Lennon:** Conceptualization (supporting); Formal analysis (supporting); Funding acquisition (supporting); Methodology (supporting); Project administration (supporting); Supervision (supporting); Writing – review & editing (supporting).

DATA AVAILABILITY

The data that support the findings of this study are available from the corresponding author upon reasonable request.

REFERENCES

- ¹U. Olsbye *et al.*, *Chem. Soc. Rev.* **44**, 7155 (2015).
- ²K. Hemelsoet *et al.*, *ChemPhysChem* **14**, 1526 (2013).
- ³A. J. O'Malley and C. R. A. Catlow, in *Experimental Methods in the Physical Sciences*, edited by F. Fernandez-Alonso and D. L. Price (Academic Press, 2017), p. 349.
- ⁴H. Jobic and D. N. Theodorou, *Microporous Mesoporous Mater.* **102**, 21 (2007).
- ⁵H. Jobic, *J. Mol. Catal. A: Chem.* **158**, 135 (2000).
- ⁶H. Jobic and A. Méthivier, *Oil Gas Sci. Technol.* **60**, 815 (2005).
- ⁷A. P. Hawkins *et al.*, *J. Phys. Chem. C* **123**, 417 (2018).
- ⁸A. J. O'Malley, S. F. Parker, and C. R. A. Catlow, *Chem. Commun.* **53**, 12164 (2017).
- ⁹A. J. O'Malley *et al.*, *Phys. Chem. Chem. Phys.* **18**, 17294 (2016).
- ¹⁰S. K. Matam *et al.*, *Catal. Sci. Technol.* **8**, 3304 (2018).
- ¹¹T. Omojola, I. P. Silverwood, and A. J. O'Malley, *Catal. Sci. Technol.* **10**, 4305 (2020).
- ¹²S. K. Matam *et al.*, *Top. Catal.* **64**, 699 (2021).
- ¹³A. L. Davidson *et al.*, *Top. Catal.* **63**, 378 (2020).
- ¹⁴I. P. Silverwood *et al.*, *AIP Conf. Proc.* **1969**, 030002 (2018).
- ¹⁵Y. Li *et al.*, *Chem. Eng. J.* **320**, 458 (2017).
- ¹⁶R. Warringham *et al.*, *J. Phys.: Conf. Ser.* **554**, 012005 (2014).
- ¹⁷A. Zachariou *et al.*, *ChemCatChem* **13**, 2625 (2021).
- ¹⁸F. Demmel *et al.*, *J. Phys.: Conf. Ser.* **1021**, 012027 (2018).

- ¹⁹Suwardiyanto *et al.*, *Faraday Discuss.* **197**, 447 (2017).
- ²⁰E. Dempsey, G. H. Kuehl, and D. H. Olson, *J. Phys. Chem.* **73**, 387 (1969).
- ²¹R. A. Jackson and C. R. A. Catlow, *Mol. Simul.* **1**, 207 (1988).
- ²²K. P. Schröder *et al.*, *Chem. Phys. Lett.* **188**, 320 (1992).
- ²³N. Raj, G. Sastre, and C. R. A. Catlow, *J. Phys. Chem. B* **103**, 11007 (1999).
- ²⁴A. J. O'Malley and C. R. A. Catlow, *Phys. Chem. Chem. Phys.* **15**, 19024 (2013).
- ²⁵A. J. O'Malley and C. R. A. Catlow, *Phys. Chem. Chem. Phys.* **17**, 1943 (2015).
- ²⁶P. P. Ewald, *Ann. Phys.* **369**, 253 (1921).
- ²⁷J. L. Banks *et al.*, *J. Comput. Chem.* **26**, 1752 (2005).
- ²⁸A. V. Kiselev, A. A. Lopatkin, and A. A. Shulga, *Zeolites* **5**, 261 (1985).
- ²⁹R. Vetrivel, C. R. A. Catlow, and E. A. Colbourn, *J. Phys. Chem.* **93**, 4594 (1989).
- ³⁰C. R. A. Catlow *et al.*, *J. Chem. Soc., Faraday Trans.* **87**, 1947 (1991).
- ³¹I. T. Todorov *et al.*, *J. Mater. Chem.* **16**, 1911 (2006).
- ³²C. W. Yong, *J. Chem. Inf. Model.* **56**, 1405 (2016).
- ³³G. Goret, B. Aoun, and E. Pellegrini, *J. Chem. Inf. Model.* **57**, 1 (2017).
- ³⁴W. G. Hoover, *Phys. Rev. A* **31**, 1695 (1985).
- ³⁵L. Van Hove, *Phys. Rev.* **95**, 249 (1954).
- ³⁶F. López *et al.*, *Phys. Rev. E* **72**, 061111 (2005).
- ³⁷B. Smit and T. L. M. Maesen, *Chem. Rev.* **108**, 4125 (2008).
- ³⁸C. T. Chudley and R. J. Elliott, *Proc. Phys. Soc.* **77**, 353 (1961).
- ³⁹P. L. Hall and D. K. Ross, *Mol. Phys.* **42**, 673 (1981).
- ⁴⁰K. S. Singwi and A. Sjölander, *Phys. Rev.* **119**, 863 (1960).
- ⁴¹H. Jobic *et al.*, *J. Chem. Soc., Faraday Trans.* **1** **85**, 4201 (1989).
- ⁴²J. Perez-Carbajo *et al.*, *J. Phys. Chem. C* **122**, 29274 (2018).
- ⁴³J. Caro *et al.*, *J. Chem. Soc., Faraday Trans.* **1** **81**, 2541 (1985).
- ⁴⁴F. Leroy, B. Rousseau, and A. H. Fuchs, *Phys. Chem. Chem. Phys.* **6**, 775 (2004).
- ⁴⁵H. Jobic, M. Bee, and A. Renouprez, *Surf. Sci.* **140**, 307 (1984).
- ⁴⁶C. L. Yaws and A. S. Y. Leh, in *Thermophysical Properties of Chemicals and Hydrocarbons*, edited by C. L. Yaws (William Andrew Publishing, Norwich, NY, 2009), p. 661.
- ⁴⁷H. Jobic, M. Bée, and G. J. Kearley, *Zeolites* **12**, 146 (1992).